Electrical protection design for integrated motor drives with carbon fibre composite casings for aircraft.

Catherine E. Jones, *Member, IEEE*, Mark Higgins, Muhammad Hijaaj Tahir, Patrick Norman and Graeme M. Burt, *Senior Member, IEEE.*

Abstract: **Replacing traditionally aluminum non-electrically active components of integrated motor drives (IMD) (e.g. casings) with lighter-weight carbon fibre reinforced polymer (CFRP) for offers a route to the key weight savings, desirable in future aircraft electric applications. However, CFRP casing designs must accommodate electrical interactions with encased equipment. Approaches to fault management and electrical protection must ensure that both electrical power system (EPS) and CFRP casing are protected against electrical faults. Knowledge of the electrical and thermal response of the CFRP casing underpins fault resilient casing design. The proposed CFRP casing is a wound filament (WF) CFRP tube for an integrated motor drive.**

This paper presents the first experimentally validated methodology to capture macro-scale electrical and thermal response of a WF CFRP tube to low frequency current. This knowledge is subsequently combined with wider EPS design considerations, including electrical grounding and bonding, to control fault response, enabling implementation of appropriate protection solutions. The results indicate that tuning casing resistance is not a viable, immediate option to control fault response, and that wider electrical system design options (grounding topologies) must be considered. Hence incorporation of CFRP for non-electrically active components to improve power density, has significant impact on wider electrical power system design.

***Index Terms*—electrical power systems, integrated motor drives, carbon fiber reinforced polymer, hybrid-electric aircraft, more-electric aircraft, all-electric aircraft.**

I. INTRODUCTION

ELECTRIFICATION of power and propulsion systems on aircraft is a key enabler for the improvement of overall aircraft efficiency, thereby reducing fuel burn and greenhouse gas emissions. This has driven the development of state-of-the-art (SOTA) more-electric aircraft (MEA), and future concepts of hybrid and all electric aircraft [1]. A parallel trend to reduce aircraft fuel burn is the use of lighter weight aircraft structures, predominantly through the use of carbon fibre reinforced polymers (CFRP). CFRP has superior mechanical properties to aluminum, and has a lower density: ~1.8 g/cm^3 for CFRP compared to 2.7 g/cm^3 for aluminum. More than 50% of structures on SOTA MEA are made from CFRP, reducing aircraft weight by ~ 20% [2], translating to a 10 – 12 % improvement in aircraft fuel burn [3].

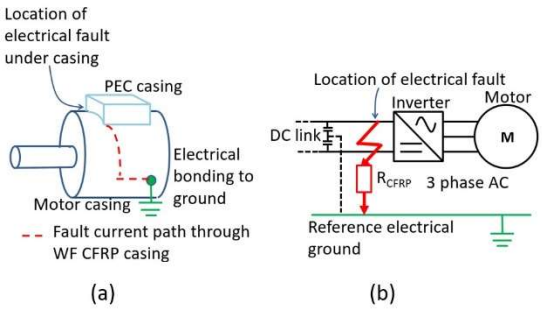

Fig. 1. (a) Fault current pathway to ground through WF CFRP tube; (b) location of the electrical fault in the EPS subsystem.

The electrification of propulsion systems necessitates an increase in power density for rotating electrical machines from ~3 kW/kg for a SOTA MEA to 10 kW/kg [1][4]. For a SOTA compact starter generator motor, 47% of the motor mass is attributable to non-electrically active components, 34 % of which is attributable to the aluminum casing [4]. Hence, a CFRP stator casing reduces casing weight by ~ 11 %.

Integrating an electrical motor with the associated power converter to form an integrated motor drive (IMD), offers further reductions in weight and volume: fewer individual casings are needed, and the amount of cabling is reduced [5][6]. The converter can either be surface mounted on the stator casing or on the end plate [6]. This paper focusses on a surface mounted topology where the converter is mounted on the stator casing of the motor, either housed as one unit, or split up into several modularized units [6].

Using CFRP for the IMD casing offers an opportunity to fully exploit the weight optimization of the IMD. The approach to casing design must consider how the casing will interact electrically with the electrical equipment. Mechanical and thermal management functionality does require consideration but is not the focus of this paper. The focus of this paper is the design of the casing, and associated electrical power system equipment (EPS), to enable timely detection, location and response of the EPS protection system to an electrical fault through the stator casing, indicated in Fig 1. Example fault scenarios include a winding to ground fault, or a rail to ground fault from the DC link to the converter or AC motor feeder. It

This paper was submitted to the IEEE transactions on Transportation Electrification for review on 16th October 2023 and accepted on 24th February 2024. This research was undertaken as part of the Rolls-Royce University Technology Centre for Electrical Power Systems at the University of Strathclyde.

All authors are with the Institute for Energy and Environment, University of Strathclyde, 204 George Street, Glasgow, G1 1RX, UK. (email: Catherine.e.jones@strath.ac.uk; mark.higgins@Strath.ac.uk; Muhammad.tahir@strath.ac.uk; Patrick.norman@strath.ac.uk; Graeme.burt@strath.ac.uk).

This is a peer-reviewed, version of record of the following paper: Jones, C. E., Higgins, M., Tahir, M. H., Norman, P., & Burt, G. M. (2024). Electrical protection design for integrated motor drives with carbon fibre composite casings for aircraft. IEEE Transactions on Transportation Electrification. Advance online publication. https://doi.org/10.1109/TTE.2024.3375932

is necessary for the IMD casing to be electrically bonded to ground to prevent the build-up of static charge on the casing [7]. The EPS protection system must respond to a fault to protect both the wider EPS and the CFRP structure from thermal degradation [8]. Other electrical interactions, outside the scope of this paper, include high frequency (>MHz) electro-magnetic interference (internally and externally generated) [9] and circulating common-mode currents (1 -2 MHz) [10].

Knowledge of the electrical properties of the casing underpin the system design trades for resilient design of both he casing, motor and wider EPS. The tubular shape of the stator results in a wound filament (WF) CFRP layup. The tube is wound with an inner and outer layer of CF and a central layer of glass fibre. For the tube in this paper, the carbon fibre is wound helically at +/- 88º to the axial direction. The glass layer provides anti-buckling functionality [11] and is wound helically at +/- 30 º. The additional stiffness provided by the glass fibre layer is necessary due to external pressure that the tube is exposed to in an aerospace application. The tube is manufactured using a wet-winding mandrel method, winding fibres in a continuous spiral around the tube [12]. The method of manufacture for the tube results in far less regular distribution of resin and fibre than for pre-preg CFRP, where mats of fibres are pre-soaked in resin prior to lay-up. The power electronics on the surface of the tube would be encased in pre-preg CFRP panels.

Limited knowledge of the macroscale (component scale) electrical and thermal response of flat, pre-preg CFRP panels is available in the published literature, *e.g.*[8], [13]-[15]. This is sufficient to capture the fault response for an electrical fault to the power electronic casing to inform initial design of compact, integrated systems [8]. However, published knowledge on electrical properties and models of WF CFRP are extremely limited [16][17]. This necessitates the development of a low frequency electrical model of the wound filament tube, to establish design criteria for an IMD with a CFRP-based casing.

The rest of this paper is structured as follows: Section II describes the electrical model which is required; Section III presents the electrical modelling hypothesis and methodology used to determine model parameters; Section IV provides validation of the modelling hypothesis; Section V presents the thermal response of the tube to Joule heating; Section VI discusses the implications of resistances estimated by the model, the electrical and thermal response of the tube for design of an IMD CFRP stator tube casing, and wider EPS design criteria; conclusions and future work are set out in Section VII.

II. Electrical Model requirements

A. Electrical model motivation and requirements

A lumped impedance model, representing the electrical resistance added by the pathway to ground through a WF CFRP tube (R_{CFRP} in Fig. 1), is needed to capture the baseline response of a stator casing to a rail to ground fault. The thermal response will inform threshold current levels for damage to the CFRP due to localized Joule heating along the conducting pathway. Combined this will inform methods to tune the response by adaption of the EPS and fault current pathway through CFRP, to enable the EPS protection system to respond appropriately to an electrical fault through CFRP.

The level of modelling fidelity required by an electrical model of a material which will interact with the EPS, is driven by the type of studies that the model is to be used for. In the EPS modelling framework presented in [18], transient fault studies are carried out using "behavioural" models, aligning to SAE AIR 6326 [19]. Thus, to ensure compatibility with the electrical power system model, the CFRP model required is a lumped resistance model, which can operate with a timestep of ~10 µs.

Ideally, the capture of the parameters for the model must minimize the need for extensive coupon testing. Analysis of a hybrid glass-carbon WF tube is presented in [17] but electrical properties are not reported.

The electrical conductivity of CF is in the range of 10's of kS/m (for polyacrylonitrile (PAN) fibre) or 100's of kS/m (for pitch fiber) [20]. Polymer resin is considered an electrical insulator. Due to the manufacturing method and high levels of pressure during the cure process, CF tows will touch through the polymer resin, creating electrical connections in both the cross-ply and through thickness directions. For a uni-directional (UD) lay-up of CFRP, the electrical resistance varies linearly with electrical resistance in the in-fibre direction. For the cross-ply and through thickness directions, the resistance of a UD [0º] layup varies inversely with length [21] .

If the electrical conductivity of the fibre and matrix, and the volume fraction of CF are known for a UD [0º] layup, the rule of mixtures can be used to theoretically estimate the electrical conductivity in the along fibre and cross-ply directions for UD lay-up [16][22],

$$\sigma_x = \sigma_f V_f + \sigma_m(1 - V_f) \quad (1)$$

$$\sigma_y = \frac{2V_f - 1}{V_f}\sigma_x \quad (2)$$

where, σ_x *(S/m)* is the electrical conductivity in the in-fibre direction, σ_f *(S/m)* is the electrical conductivity of the CF, σ_m *(S/m)* is the electrical conductivity of the resin matrix, V_f is the volume fraction of fibre to resin (typically around 0.55 – 0.58), σ_y *(S/m)* is the cross-ply electrical conductivity.

However, in a WF layup with a helical winding pattern, the tows do not align directly to the *x* (hoop) and *y* (axial) axes, due to the variation in angle of the CF tows around the tube [12][16]. Approaches to capture the influence of fibre angle on electrical properties have been investigated for pre-preg CFRP. In [23], the electrical conductivity for a ply where fibres are orientated such that they are not aligned to the x-axis is given by

$$\sigma_\theta = \sigma_x \sin^2\theta + \sigma_y \cos^2\theta \quad (3)$$

where θ is the angle that the fibres are arranged relative to the x-axis, and σ_θ *(S/m)* is the electrical conductivity at the angle θ. However, [16] shows that (3) does not correlate well with experimental results because it does not include the influence of inter-ply connections. A linear relationship between ply angle and electrical conductivity is proposed in [16]. An empirical-based formula is given in [24], but is specific to a

particular layup, so does not translate to different layups. A lumped impedance model of a quasi-isotropic (QI) (multi-direction fibre orientation) CFRP layup is described in [8] but is not validated.

An alternative approach for QI layups is to develop a macro-scale model by extrapolation of electrical conductivity in *x, y* and *z* directions from a microscale (fibre and resin level) or a mesoscale (ply level) to the macro scale, e.g. [13][14]. However the resulting macroscale model is too computationally complex for compatibility with a behavioral EPS model. Further, the methods are for a panel of CFRP, which has edges where the CF discontinues. In contrast, in a wound filament tube, the tows of fibre are continuous for the full component, as they spiral around the tube. As such, methods which require extensive use of coupons to estimate electrical properties in the axial direction (for a hoop wound tube) will remove the continuity of the fibre in the hoop direction. Coupons are test specimens of a layup, which are used to determine material properties. Coupon dimensions are determined based on the test being undertaken. The level of influence that this would have on the cross-ply conductivity is unknown. Hence using coupons to estimate this property for a WF layup is not desirable.

B. Thermal response of CFRP due to Joule heating

Limited studies on the thermal response of CFRP due to localized Joule heating are presented in the literature. A correlation between time taken to reach the glass transition temperature (T_g) of epoxy resin and power dissipated due to conduction of electrical current through a UD [0º] layup is presented in [8]. Correlation between distribution of electrical current in the CFRP with exit and entry points, and associated variation in temperature due to Joule heating is presented in [25] for pre-preg laminate. Degradation due to localized heating is documented in [26]. However, the thermal response of a WF CFRP tube with glass fibre reinforcement due to Joule heating is not presented.

III. Modelling Hypothesis and Methodology

A. Modelling hypothesis

The electrical properties between two points on the surface of the WF CFRP tube are determined by the pathway taken by electrical current through the tube, which from the literature discussed in Section II, is sensitive to CFRP layup. For the WF CFRP tube investigated for this paper, the inner and outer layers of CFRP are each 0.425 mm thick and consist of pitch CF tows (Mitsubishi Dialead K13916 [27]) with 16,000 fibres in a tow. The tows are laid up at +/- 88º (relative to the axial direction), held in place by an epoxy resin (Araldite LY 5210), which has a glass transition temperature (T_g) of 180 ºC[28]. Inner and outer layers of CFRP are separated by a 0.640 mm layer of glass fibre, laid up at +/- 30º. The angle of the winding for the glass and carbon fibres was chosen to optimize the mechanical properties, in particular the stiffness, of the tube. The volume fraction of CF in the CFRP layers was provided by the tube manufacturers and stated to be ~ 0.55 in the hoop direction. The final tube has an outer circumference of 932 mm, length of 447mm and a total thickness of 1.49 mm. All tube parameters are summarized in in the Appendix. Two tubes were used for the experimental work in this paper. The first was tested as a complete tube, the second was used to provide smaller samples.

If an electrical current is injected between points A and B on a tube, as indicated in Fig. 2, then due to the high electrical conductivity of CF compared to the resin, most of the electrical current will flow along the fibres to the exit point. It is proposed that this is represented in a model as one continuous pathway, which spirals around the tube going from point A to point B (which are both positioned on the outside surface of the tube), as indicated by the blue line in Fig. 2. By inspection of the surface of the tube in Fig. 3, the irregularity of the composition of the tube is evident, including irregular CF tow-to-CF tow contact in the axial direction. These connections are indicated by the red lines in Fig. 2. To validate these assumptions a low current (<1A) was injected between two points on the surface of the tube. The sections of tube conducting electrical current and the associated dissipated heat due to Joule heating are indicated in Fig. 4. This verifies that the full area between the entry and exit electrodes is conducting electrical current.

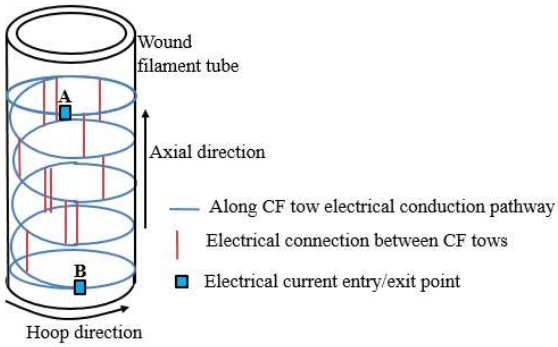

Fig. 2. Proposed conducting pathway between two points, A and B.

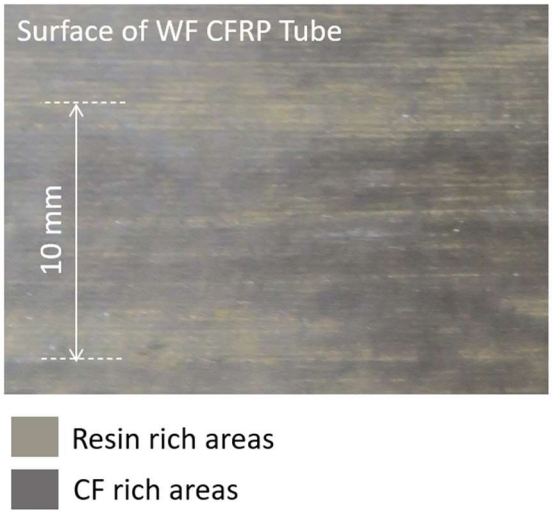

Fig. 3. Photograph of the outer surface of the tube showing visible evidence of connections between CF tows in the axial direction on the surface of the tube.

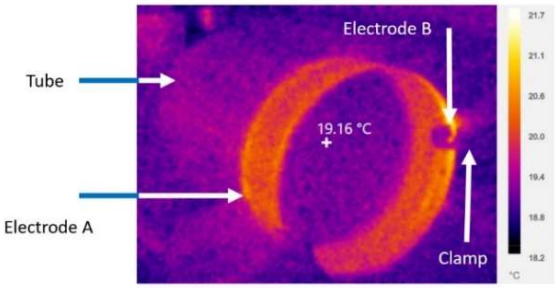

Fig. 4. Thermal image indicating the pathway taken by electrical current through CFRP, between two points, A and B.

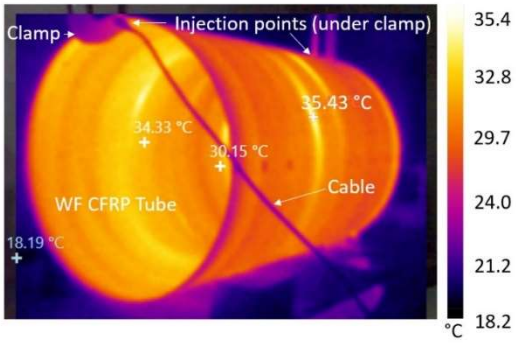

Fig. 5. Thermal image of tube indicating hotspots due to electrical connections between inner and outer layers of CFRP.

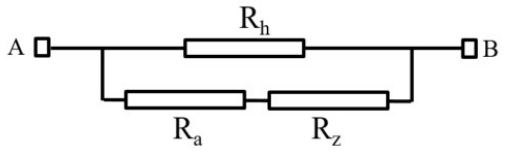

Fig. 6. Proposed lumped impedance model.

Theoretically, the inner and outer layers of CFRP are electrically isolated by the glass fibre layer. An electrode was placed on the inner surface of the tube, and a second electrode on the outer surface of the tube. To apply electrodes, 10 x 10 mm squares of the surface of the tube were sanded using fine grit (320 gsm) sandpaper to smooth the surface and expose the outermost layer of CF [8]. To minimise contact resistance, silver epoxy was applied, and a piece of copper foil was clamped to the electrode using a vice [8]. Kelvin probes were clipped to the copper foil. An LCR meter was used to measure the electrical impedance at 100 Hz. A resistance of 30 Ω was measured, which indicates carbon fibres from the inner and outer layers of CFRP touching through the glass fibre layer. A current of 1.5 A was injected between two electrodes which were positioned on the outer surface of the tube at opposite ends. The variation in tube surface temperature is visible in Fig. 5. The hot spots are due to tows of CF on the inner and outer surfaces of the tube physically touching each other through the glass layer. These connections form during the manufacturing process, where the resin matrix is cured by placing the tube in an autoclave and applying a high pressure. As a result, electrical current is conducted through a small cross-sectional area at these electrical contact points between the inner and outer CF layers.

The electrical response of the tube over the frequency range from 0 to 10 MHz was performed using a spectrum analyser with two electrodes positioned at opposite ends of the tube. Results indicated the behaviour was purely resistive below frequencies of 20 kHz. At 100kHz the tube exhibits a small amount of inductive behaviour with a phase angle of 5°. Hence for investigation of the electrical properties at low frequencies, the tube was treated as purely resistive.

Based on these observations, a lumped impedance model is proposed in Fig. 6, where the electrical resistance is composed of a hoop component, R_h *(Ω)* an axial component R_a *(Ω)* and a through thickness component R_z *(Ω)*. R_z is due to the electrical connections between the outer and inner layers of CFRP through the glass fibre layer. The total electrical resistance between points A and B, R_T *(Ω)* is given by

$$R_T = \frac{R_h(R_a+R_z)}{R_h+(R_a+R_z)} \quad (4).$$

Once electrical resistances are known, then electrical conductivities in the hoop and axial directions can be estimated using

$$R_h = \frac{l_h}{\sigma_h A_h} \quad (5)$$

$$R_a = \frac{l_a}{\sigma_a A_a} \quad (6)$$

where l_h *(m)* and l_a *(m)* are the length in the hoop and axial directions, σ_h *(S/m)* and σ_a *(S/m)* are the electrical conductivity in the hoop and axial directions, and A_h *(m²)* and A_a *(m²)* are the cross-sectional conducting area in the hoop and axial directions.

B. Methodology to capture model parameters

In-fibre (hoop) direction electrical properties of CFRP are expected to behave linearly with distance [8], and are expressed as

$$R_{ht} = r_{hm} l_h + R_c \quad (7)$$

$$R_h = R_{ht} - R_c \quad (8)$$

where R_{ht} *(Ω)* is the total resistance measured, r_{hm} *(Ω/m)* is the resistance in the in-fibre (hoop) direction per metre, and R_c *(Ω)* is the contact resistance. The length, l_h, is calculated by estimating the number of loops of CF around the tube between the entry and exit points, given by

$$l_h = \frac{l_a}{b} C \quad (9)$$

where *b (m)* is the length of the entry point in the axial direction, *C (m)* is tube circumference.

Measuring between two points aligned in the hoop direction on the tube is effectively measuring across a parallel resistance, due to the continuous winding of CF around the tube. Hence, to estimate a value for r_{hm} and R_c, strips of tube in the hoop direction were cut from a second tube, the same layup as the first. The strips were 47 mm, 65 mm, 83 mm, 103 mm and 123

mm wide. An example strip of tube, prepared with electrodes is shown in Fig. 7. Electrodes were prepared as described in Section III A. Six pairs of electrodes were placed on each strip, to accommodate irregularities in the layup between different measurement points.

The values for axial resistance and conductivity cannot be estimated from strips of tube: to do so would overlook the influence of the continuous nature of the electrical conduction pathway in the hoop direction. The axial and through-thickness parameters between two points on the tube's surface were estimated by measuring the resistance between points vertically aligned in the axial direction (Fig. 8), and applying

$$R_{az} = \frac{R_h R_T}{R_h - R_T} = r_{am} l_a + R_z \quad (10)$$

where R_{az} *(Ω)* is the combined series resistance of R_a and R_z, R_h *(Ω)* is hoop direction resistance, and r_{am} *(Ω/m)* is the variation in resistance in the axial direction with axial length (l_a *(m))*. By plotting R_{az} against l_a, the value of R_z can be extracted from the intersection with the *x*-axis at 0 m. The gradient of the line indicates the value of r_{am} and (6) was used to estimate $\sigma_{a.}$.

For measurements in the axial direction, 10 x 10 mm silver paint electrodes were placed on the wound filament tube spaced by a quarter of the circumference around the outer surface of the tube. No electrodes were placed more than 110 mm from the tube ends due to limitations on jaw sizes of the lightweight, aluminum clamps used in the measurement process. Larger, heavier clamps were not used to avoid the possibility of structural distortion, which would affect the electrical properties [21].

IV. Validation of Electrical Modelling Hypothesis

A. Estimation of model parameters

Fig. 10 shows the median values for the measured values of R_h against hoop distance. By inspection, and application of (7), r_{hm} is estimated to be 9.5 Ω/m. By extrapolating this line of best fit back to the y-axis, the contact resistance is estimated to be 0.02 Ω, which is comparable to values for contact resistance reported in the literature [8]. For the hoop direction, the cross-sectional conducting area is the thickness of the CFRP outer or inner CFRP layer, (0.425 x 10^{-4} m) multiplied by the axial length of the injecting electrode (0.01 m). Hence the cross-sectional conducting area in the hoop direction is 4.25 x 10^{-6} m. Hence, from (5), the electrical conductivity in the hoop direction was estimated to be 24.7 kS/m.

To estimate values for R_a, σ_a and R_z, the median values for R_{az} are plotted against axial distance in Fig. 11 r_{am} *(Ω/m)* is estimated to be 35.2 Ω/m and R_z *(Ω)* estimated as 0.95 Ω. The cross-sectional conducting area in the axial direction is given by the multiplication of cross-sectional area of the CF layer of the tube (0.425x10^{-3} m) and the tube circumference (0.932 m). Applying (6), this gives a median conductivity for the axial direction of 69.9 S/m.

Although the electrical conductivity of the tube is much higher in the hoop direction compared to the axial direction, the larger cross-sectional conducting area and much lower distance (l_a compared to l_h) in the axial direction, results in an electrical resistance an order of magnitude lower in the axial direction compared to hoop direction. Hence R_T is dominated by R_a.

B. Model validation

To validate the model, measurements were taken between electrodes which were offset in both the axial and hoop directions. Electrodes were offset in the hoop direction by either a half or quarter of the circumference of the tube. Due to the dominance of R_a over R_h when estimating R_T, estimated and measured resistances were plotted against axial distance between electrodes.

The estimated values σ_a, σ_h and R_z extracted from results presented in Section IV-A were used to calculate the electrical resistance between two points on the surface of the tube. For the hoop direction, (5) is applied. The hoop length, l_h, is given by (9). To calculate R_h (5) was applied. R_z was taken as the constant 0.95. Measured and calculated values for R_T are compared in Fig. 12. For each additional offset of a quarter of the circumference of the hoop between electrodes, R_h increased by 2.21 Ω. This had a very low influence on total resistance, as R_h is an order of magnitude higher than R_a. The correlation between the estimated and measured results is on average within 5 %.

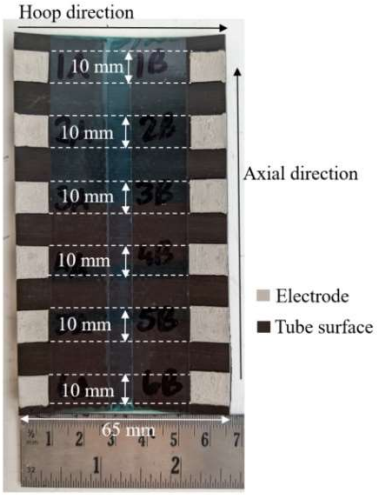

Fig. 7. Example strip of tube for measuring the resistance in the hoop direction.

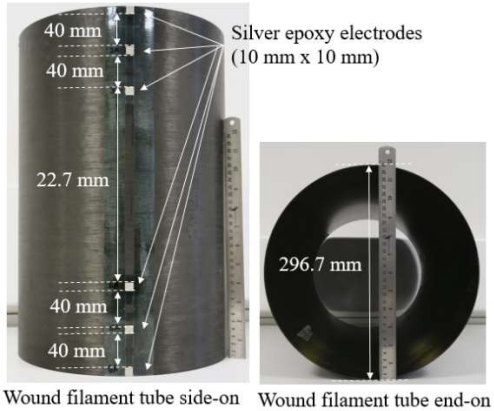

Fig. 8. Position of electrodes to measure resistance between two points on the surface of the tube.

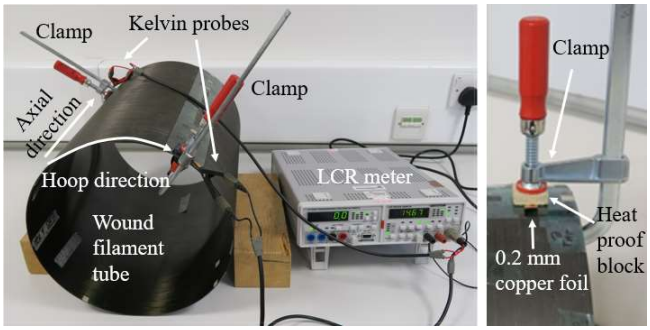

Fig. 9: Left hand side: full set-up with LCR meter, kelvin probes and tube. Right hand side: detail of the connection to the electrodes on the surface of the tube.

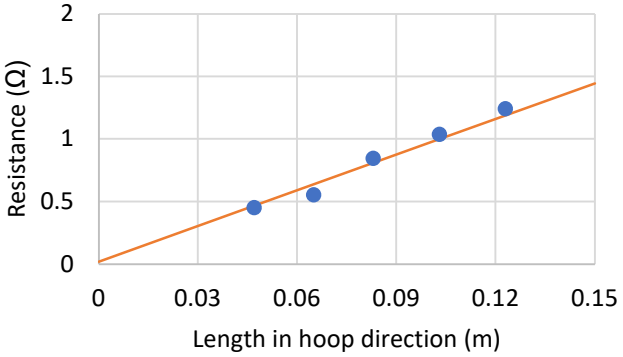

Fig. 10. Median measured values of R_h (Ω) against hoop length (blue) and line of best fit (orange) to extract r_{hm} (Ω/m), and contact resistance (Ω).

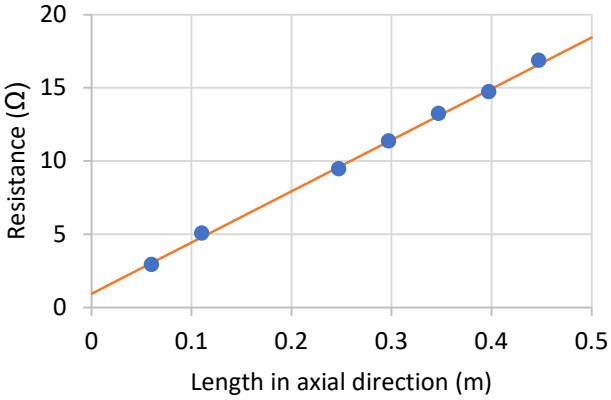

Fig. 11. Median measured values of R_{az} (Ω) against axial length (blue) and line of best fit (orange) to extract r_{az} (Ω/m), and R_z (Ω).

By inspection of Fig. 12, the total resistance between two points on the tube (with electrodes that are 10 mm x 10 mm) can be expressed by

$$R_t = 35l_a + 0.8699 \qquad (11).$$

R_t is included on Fig. 12 as the green line.

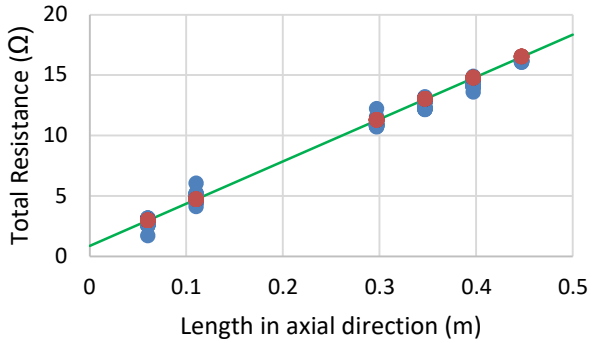

Fig. 12: Comparison of measured value of resistance (blue), calculated resistance from conductivity and R_z values (orange) and from (11) (green).

V. Thermal Response

To assess the thermal response of the tube, current was injected through the electrodes aligned in the axial direction at the far ends of the tube. The current level was increased in 0.5 A steps, starting from 1A, increased once temperature reached a steady state. The temperature at the injection point was measured using a thermocouple, with temperature across the full tube monitored using a thermal camera. Prior to heating, resistance for the full length of the tube was 16.8 Ω. Results are given in Fig. 13. The resistance of the CFRP has a negative temperature coefficient, and hence resistance drops as the CFRP heats up due to localized Joule heating from current conduction [15] . Up to an injected current of 3.5 A, the resistance of the tube drops by approximately 2-3% (~0.5 Ω) of the total resistance, as the temperature increases and then reaches a steady state. At 3.5 A, the temperature measured at the input electrode of the tube reaches a maximum of 70 ºC, well below T_g of the epoxy resin (180 º C). When 4 A is injected, the temperature at the entry point reaches 90ºC, but the measured resistance does not reach a steady state, and continues to decrease with time.

Images taken from the thermal camera (Fig. 5 and Fig. 14) indicate that the hottest area of the tube during electrical conduction are not at the entry and exit points of the electrical current. The results indicate that hotspots occur in the conducting pathway between the entry and exit points and these are due to electrical connections between CF through the central glass fibre layer. The maximum hot spot temperature observed before the 4A test was stopped was 166 ºC; Fig. 14 shows a hot spot at 153.09 ºC. The sharp decrease in resistance at 3800 s in Fig 4 indicates a rapid change in electrical properties, caused by localised thermal degradation at a hotspot, and indicates that glass transition temperature was reached. On inspection of the tube once cooled to room temperature, scorch marks were observed on the tube at the location of hotspots, and the measured resistance had increased from 16.8 Ω to 18.6 Ω, further indicating that localized heating had resulted in glass transition temperature being reached resulting in damage to the tube.

VI. Discussion

A. Assessment of electrical and thermal response of the tube.

The levels of electrical conductivity estimated for the hoop (24.7 kS/m) and axial (69.9 S/m) directions, are comparable to values for other layups of CFRP in the literature. In [17] a hoop wound tube (with no glass fibre layer), with a volume fraction of fibre at 75%, had a conductivity of 47.5 kS/m in the hoop direction and 70 S/m in the axial (transverse) direction. In [16] the conductivity for a hoop wound at +/- 75°, and measured at an angle of 15° to the winding direction, was estimated to be 21.7 kS/m. The tube in this paper is wound at +/- 88 °, with a volume fraction of CF to resin of 55%. The type of CF used in [16] is not stated; this will impact on the results as PAN fibre is ~10 times less electrically conductive than pitch fibre. In-fibre conductivity values in [17] are high, but the volume fraction of fibre is high (70%). However, the value for the transverse (axial) direction conductivity is very similar to results obtained for this paper.

Applying (1), with the electrical conductivity of the carbon fibre (0.196 MS/m) and V_f of 55%, returns a hoop direction electrical conductivity of 107.8 kS/m. This is far higher than the experimentally estimated value of 27 kS/m. Using (1) to estimate equivalent V_f of the tube, returns 14 %. The WF tube is much less uniform in layup than a uni-directional panel of CFRP, and carbon fibres are aligned at +/- 88 °. Hence further investigation on adaption of (1) to generalize the hoop direction electrical characteristics is needed. This will subsequently enable generalization of the axial direction conductivity (equivalent of σ_y) from (2), which is dependent on axial conductivity (equivalent of σ_x) from (1).

Application of (5) – (10) to extract the electrical characteristics of the tube, to enable resistance calculation using (4) gives an estimation of tube resistance to within 5%. This is sufficient for assessing the influence of the CFRP resistance on electrical fault response.

Results in this paper indicate that the glass fibre layer has a low impact on total resistance. However, it does heavily influence the level of current that the hoop can conduct a current without the occurrence of localised thermal degradation, due to the irregular electrical connections between the inner and outer layers of carbon fibre through the central glass fibre layer.

Total hoop resistance (R_T) is dominated by the axial component. The hoop electrical conductivity is multiple orders of magnitude higher compared to axial direction conductivity. However the hoop resistance is much higher than the axial resistance due to the longer distance travelled by current in the hoop direction, combined with a smaller cross-sectional conducting area compared to the axial direction. The component R_z, attributed to electrical contacts made through the glass fibre layer, is not insignificant. If this component is neglected, the average error between estimated and measured resistance between two points rises to 15 %. At lower values of resistance, this may be sufficient to prevent an accurate assessment of fault response in a simulation based study.

The dominance of R_a reduces the sensitivity of the lumped tube resistance to the area of the injection point on the surface of the tube: a smaller injection point will result in a smaller cross-sectional conducting area in the hoop direction, but cross-sectional conducting area in the axial direction is unaffected. This is demonstrated in Fig. 15 which compares the measured resistance between two points on the tube where the length of the electrode in the axial direction is reduced from 0.01 m to 0.05 m. Hoop resistance for the smaller electrode is ~4% higher than for the larger electrode.

B. Fault Management Strategy Approaches

From the electrical and thermal characteristics of the tube presented in Sections III and IV, three fault management methods for the case of a rail to ground fault through the hoop have been identified and are summarized in Table 1.

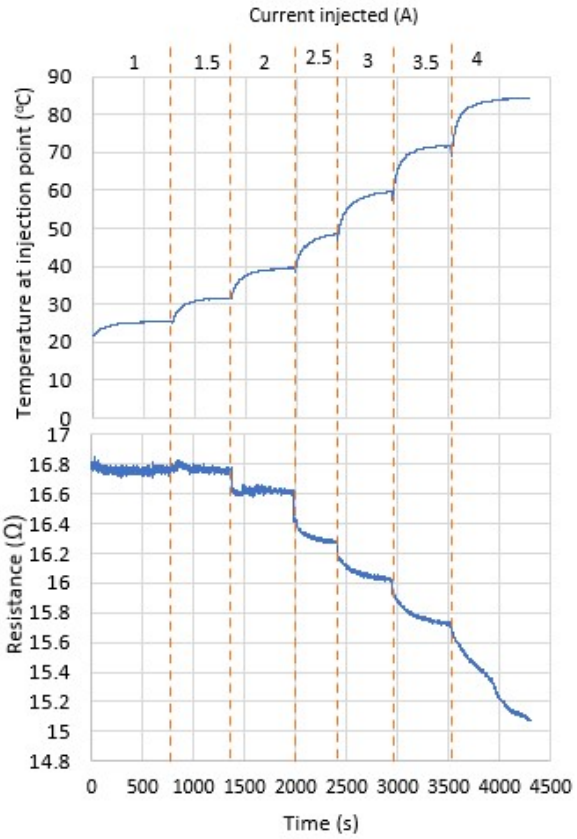

Fig. 13: Variation of tube resistance and temperature with different levels of injected current.

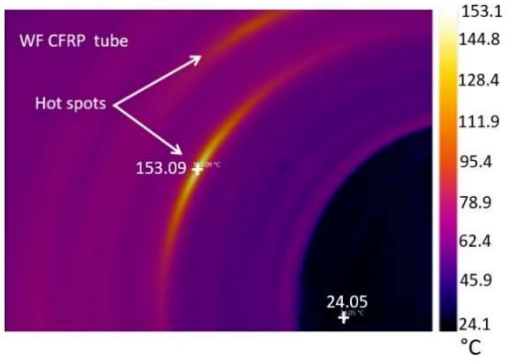

Fig. 14: Hot spot approaching glass transition temperature on inside of tube, with 4 A injected.

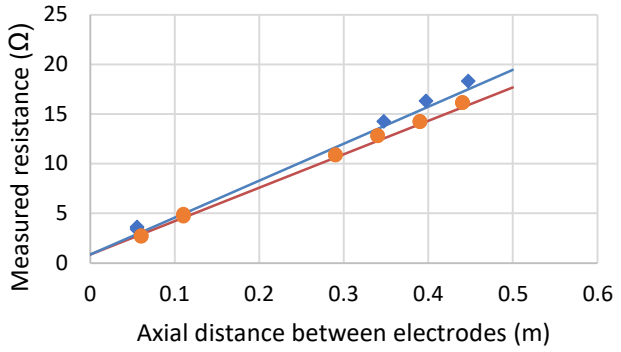

Fig. 15. Sensitivity of resistance to cross-sectional area of surface electrodes: measured values from 5 x 10 mm electrodes (orange circles), 10 x 10 mm electrodes (blue diamonds), and calculated values using the model for 5 x 10 mm electrodes (blue line) and 10 x 10 mm electrodes (orange line).

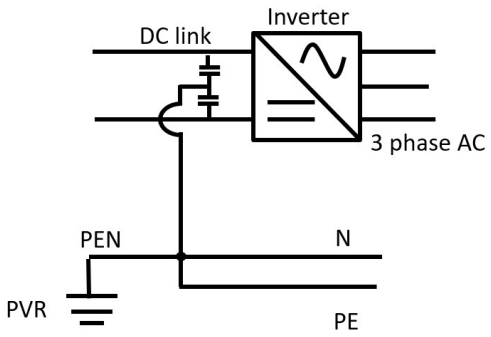

Fig. 16: High level schematic of TN-C-S grounding system, showing neutral (N), protective earth (PE), combined neutral and protective earth (PEN) and the point of voltage reference (PVR).

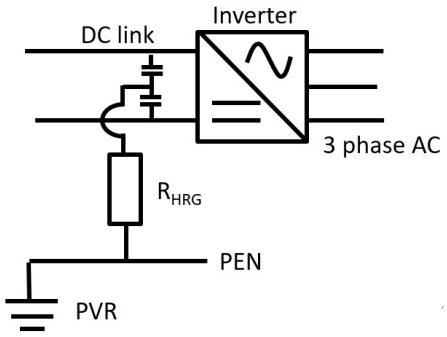

Fig. 17: High level schematic of HRG grounding system., showing the grounding resistance, R_{HRG}, between the neutral point and the PEN, which is connected to the PVR.

A significant design threshold is the level of current that the tube can conduct before thermal degradation occurs. For the tube investigated in this paper, this is 3.5 A. Hence the electrical protection system must respond appropriately before degradation occurs. The first option in Table 1 is to restrict the fault current to be less than the threshold current for thermal degradation. One method to achieve this is to have a TN-C-S ("T" is for Terre and indicates a low resistance connection to protective Earth (in an aircraft Earth is a point of voltage reference (PVR) at the front of an aircraft [30]); "N" indicates grounding a neutral wire; "C-S" indicates that neutral and protective Earth are separate and then combined). For safety reasons, protective earth and neutral are kept separate within the aircraft cabin, but are combined elsewhere to reduce weight [31]. The neutral point of the system may be the electrical generator, but this can be difficult to physically access. Hence in Fig. 16 the neutral point is taken as the mid-point of the DC link. If TN-C-S is chosen, design the physical layout of the electrical components on the stator casing in the IMD such that the location of an electrical fault will provide sufficient. electrical resistance to limit the fault current. The advantage of TN-C-S is that it is the grounding topology used for SOTA aircraft EPS [31], and hence legacy equipment and systems are designed for this grounding topology.

As discussed, R_T is dominated by axial resistance. Hence, the axial length of the hoop limits the maximum value for R_T. Accordingly, ensuring the distance travelled by fault current in the axial direction is high enough to ensure a high enough resistance to limit fault current is unlikely to be a viable option. For example, for an 80 kW motor, with a rail to ground fault from a +270 Vdc rail through the CFRP casing, a fault resistance of at least 77 Ω would be required. The maximum resistance that can be added by the tube studied is ~16.8 Ω.

A second option to limit fault current is to implement a high resistance grounding (HRG) topology (Fig. 17). In a HRG topology, the neutral point of the electrical power system is grounded through a resistor. The resistor is sized to limit fault current, as outlined in [32].The advantage of this approach is that the fault current is decoupled from fault resistance, and hence tube size and physical location of a fault. Hence this approach allows for flexibility in tube size and geometry, positioning of equipment and position of electrical bonding points on the hoop. The bonding points will be bolts, which will have an influence on the mechanical properties of the tube. Hence it allows for optimization of tube design for design criteria other than electrical failure modes. For a rail to ground fault in an HRG topology, due to the change in magnitude of the neutral voltage relative to ground in the event of a fault, the fault must be cleared before a second fault occurs, to prevent the occurrence of a double rail to ground fault. The change in neutral voltage indicates that an electrical fault to ground has occurred, but locating the fault is challenging [33]. Fault location methods based on frequency spectrum analysis may offer a solution, e.g. [34]. However, these have yet to be experimentally verified for a noisy, aircraft EPS environment [29]. An IT grounding topology (where the intention is to not connect electrical conductors to ground [32]) has not been considered due to the uncontrolled, high transient over-voltages which are likely to occur due to parasitic capacitances between electrical equipment and the casing [33] [35].

The third option is to control the fault resistance to be sufficiently low for conventional under current and over voltage protection methods to be implemented. A solid grounding topology must be used, hence TN-C-S can be used. To implement this method, the location of the electrical fault relative to the bonding point to ground must be controlled such

TABLE I
SUMMARY OF DESIGN OPTIONS FOR CFRP CASINGS FOR IMD FOR ELECTRICAL FAULT DETECTION.

Design Option	Method	Advantages	Disadvantages
1. Limit fault current to below threshold for thermal degradation.	Minimise axial distance between fault location and electrical bonding point on tube.	Can operate with a TN-C-S grounding topology. Provides fault ride through capability.	Amount of resistance added by CFRP is limited by tube axial length.
	Implement high resistance grounding topology	Decouples electrical fault impedance from fault response: • Insensitive to physical location of fault to bonding. • Design flexibility for physical location of equipment, electrical bonding points on the tube and tube geometry and layup.	Must clear a fault once it occurs to prevent occurrence of second rail to ground fault. Fault location (if required) can be difficult.
2. Control fault resistance to be low enough for over current protection methods.	Ensure axial distance between fault location and electrical bonding point on tube is below threshold.	Enables deployment of conventional over-current protection with a solidly grounded system and use of TN-C-S grounding topology.	Restricts topology of IMD design by restriction of physical location of equipment on tube surface and electrical bonding points.

that the fault current will result in a change in the measured system current of at least 10 %, ideally 20 %.

The disadvantages of this approach are that it will require the co-design of the location of connectors and cables where faults are likely to occur with location of electrical bonding points on the tube. As for the first option, physical location of these elements may be interdependent on other factors such as connection to the wider EPS, and impact on mechanical integrity of the tube.

Achieving a low enough electrical resistance is possible. For example, the level of resistance required to ensure a 20% change in DC link current for a rail to ground fault from a 270 Vdc rail for an 80 kW electrical motor is ~4.6 Ω. This corresponds to a distance of ~0.11 m for the tube investigated in this paper. The fault current would be ~59 A. The protection system must be able to locate and detect this fault before the CFRP thermally degrades; either at a hot spot, or if hotspots can be eliminated by changes to the manufacturing process, due to heating of the full conducting section of the CFRP tube. Considering the results in this paper, and in [8], it is expected that the protection system would need to detect, locate and isolate the fault within a few seconds.

VII. CONCLUSIONS

WF CFRP tubes, with a glass fibre layer for anti-buckling functionality, offer a route to for a lightweight IMD casing. For an IMD operating in a hazardous environment on board an aircraft, the case of a short circuit to ground through the CFRP casing must be considered for casing and associated EPS design.

From the analysis presented, it is the axial distance between two points on the surface of the tube which significantly impacts tube resistance. The threshold level of current which can be conducted is limited by the irregular connections between the inner and outer layers of CF through the central glass fibre layer.

The most attractive approach for the resilient design of an IMD with a CFRP casing in the near term is a high resistance ground (HRG) grounding topology. The fault current cannot be limited using the CFRP tube: even if the tube was long enough for a high enough resistance to be possible, the constraints on location of electrical equipment and electrical bonding points to ground may be too restrictive. Future investigations are needed to determine how precisely a fault location needs to be identified for an HRG topology, and to experimentally validate methods to achieve this for next-generation aircraft.

Two barriers are evident for the approach of ensuring the pathway to ground through the tube has a low enough resistance to enable a TN-C-S grounding topology with implementation of over-current based protection. The first is the hot-spots caused by irregularities in the manufacture of the tube where the outer and inner CF touch through the glass-fibre layer. This requires further analysis to determine how fast the glass transition temperature of the polymer resin will be reached at higher currents than those studies in this paper. Research into manufacturing methods to control or predict or even eliminate these imperfections, is also needed, to enable design thresholds to be used for different tubes of the same layup. The second barrier to implementation of this method is the restrictions in wider design flexibility (location of equipment, location of bonding points).

Whilst this paper has focused on the electrical requirements of the WF CFRP stator casing for low frequency (<MHz) interactions, further investigation into higher frequency interactions for common-mode currents (MHz) and EM shielding, and formation of eddy currents in the casing, is also needed. Investigation is also needed into the potential thermal management functionality a WF CFRP casing, and the potential subsequent impact on electrical functionality.

This paper has demonstrated the estimation of resistance between two points on the surface of the tube to within 15 % of the measured resistance, with knowledge of hoop and axial electrical conductivity and thickness of carbon fibre layers. With specific knowledge of the through thickness direction resistance (due to irregular carbon fibre contacts through the glass layer) resistance can be estimated to within 5% of the measured resistance. Further work is needed to correlate sensitivity of through thickness resistance levels to tube layup variables and dimensions, and whether adapting the manufacturing process can eliminate irregular electrical connections between the inner and outer layers of carbon fibre through the central glass fibre layer.

APPENDIX

TABLE 2
SUMMARY OF PARAMETERS FOR THE WF CFRP TUBE PRESENTED

Tube Parameter	Value
Carbon fibre tows	Mitsubishi Dialead K13916, 16k fibres per tow.
Epoxy resin	Araldite LY 210
Glass transition temperature of epoxy resin	180 ºC
Angle of winding of carbon fibre	+/- 88 º relative to axial direction
Angle of winding of glass fibre	+/- 30 º relative to axial direction
Tube length	447 mm
Tube circumference	932 mm
Thickness of each carbon fibre layer	0.425 mm
Thickness of glass fibre layer	0.640 mm
Estimated electrical conductivity in axial direction, σ_a	69.9 S/m
Estimated electrical conductivity in hoop direction, σ_h	24.7 kS/m
Estimated resistance in through thickness direction, R_z	0.95 Ω

ACKNOWLEDGEMENT

The authors acknowledge preliminary measurements of the electrical resistance of the WF CFRP tube taken by Mr Ciaran Duguid, and the support of Mr Richard Munro with the experimental set-up in the laboratory.

VII. REFERENCES

[1] J. Benzaquen, J. He and B. Mirafzal, "Toward More Electric Powertrains in Aircraft: Technical Challenges and Advancements" CES Transactions on Electrical Machines and Systems, Vol. 5, No. 3, pp. 177 – 193, 2021, doi: 10.30941/CESTEMS.2021.00022.

[2] "Boeing 787: From The Ground Up", Aero, Boeing, qtr 4, 2008, Accessed on: 29th May 2023, [Online]. Available: https://www.boeing.com/commercial/aeromagazine/articles/qtr_4_06/article_04_2.html

[3] M. Marino and R. Sabatini, "Advanced lightweight aircraft design configurations for green operations", *Practical Responses to Climate Change Conference*, Engineers Australia, 2014.

[4] G. Jewell, "Light-weighting in Electrical Machines – Opportunities and Challenges", *Future Electrical Machines Manufacturing Hub Lightweighting Conference*, 2019, Accessed on 29th May 2023, [Online]. Available: https://electricalmachineshub.ac.uk/outputs/presentations/

[5] S. Wu et al, "Design and Analysis of an Integrated Modular Motor Drive for More Electric Aircraft", *IEEE Trans. on Transportation Electrification*, Vol. 6, Issue 4, pp 1412 -1420, 2020, doi: 10.1109/TTE.2020.2992901.

[6] W. Lee et al, "A Review of Integrated Motor Drive and Wide-Bandgap Power Electronics for High-Performance Electro-Hydrostatic Actuators", *IEEE Trans. on Transportation Electrification*, Vol. 4, Issue 3, pp 684- 693, 2018, doi: 10.1109/TTE.2018.2853994

[7] "AC 43.13-1B Acceptable Methods, Techniques, and Practices – Aircraft Inspection and Repair", Federal Aviation Administration, 1998, Accessed on 29th May 2023, [Online]. Available: https://www.faa.gov/documentlibrary/media/advisory_circular/ac_43.13-1b_w-chg1.pdf.

[8] C.E. Jones et al, "Electrical and Thermal Effects of Fault Currents in Aircraft Electrical Power Systems with Composite Aero-Structures", *IEEE Trans. on Transportation Electrification*, Vol. 4, Issue 3, pp 660 - 670, 2018, doi: 10.1109/TTE.2018.2833838.

[9] C.E. Jones et al, "A Route to Sustainable Aviation: A Roadmap for the Realization of Aircraft Components with Electrical and Structural Multifunctionality", *IEEE Trans. on Transportation Electrification*, Vol. 7, Issue 4, pp 3032 – 3049, 2021, doi: 10.1109/TTE.2021.3078118.

[10] M. Schuster, J. Springer and A. Binder, "Comparison of a 1.1 kW Induction Machine and a 1.5 kW PMSM Regarding Common-Mode Bearing Currents", IEEE International Symposium on Power Electronics, Electrical Drives, Automation and Motion, 2018, doi: 10.1109/SPEEDAM.2018.8445298.

[11] A.T. Read, S. Hua and R. Butler, "Damage Resistance and Damage Tolerance of Hybrid Carbon-Glass Laminates" Composites Part A: Applied Science and Manufacturing, Vol. 76, pp. 224 – 232, 2015, doi: 10.1016/j.compositesa.2015.06.001.

[12] M. Quanjin et al, "Design and Optimize of 3-axis Filament Winding Machine", *IOP Conference Series: Materials Science and Engineering*, Vol. 257, 2017, doi: 10.1088/1757-899X/257/1/012039.

[13] F. Senghor et al, "Electrical conductivity tensor modeling of stratified woven-fabric carbon fiber reinforced polymer composite materials", *IEEE trans. on Magnetics*, Vol. 53, Issue 6, 2017, 10.1109/TMAG.2017.2660529

[14] A. Piche, I. Revel and G. Peres, "Experimental and numerical methods to characterize electrical behavior of carbon fiber composites used in aeronautic industry", *Advances in Composite Materials-Analysis of Natural and Man-Made Materials, IntechOpen*, 2011.

[15] J. B. Khan et al, "Experimental characterization of carbon fiber composites for use in future aircraft applications", *IET Science, Measurement & Technology*, Vol. 13, Issue 8, pp. 1131-1138, 2019, 10.1049/iet-smt.2018.5601

[16] A.S. Kaddour, F.A.R. Al-Salehi and S.T.S Al-Hassani, "Electrical resistance measurement technique for detecting failure in CFRP materials at high strain rates", *Composites Science and Technology*, No. 51, pp. 377-385, 1994.

[17] G. R. Headifen and F. P. Farenthold, "Mechanical and electrical properties of glass and carbon fiber reinforced composites", *ASME Energy-Sources Technology Conference*, 1989.

[18] C.E. Jones, P. J. Norman and G.M. Burt, "A Modelling Framework for Efficient Design of Electrical Power Systems for Electrical Propulsion Aircraft", *AIAA/IEEE Electric Aircraft Technologies Symposium*, 2021.

[19] "SAE AIR 6326: Aircraft Electrical Power Systems Modeling and Simulation Definitions", SAE International, 2015.

[20] -,"900GPa – Worldwide Hub for composite materials", [online]. Available: https://www.900gpa.com/en?u=metric

[21] J.C. Abry et al, "In situ detection of damage in CFRP laminates by electrical resistance measurements", *Composites Science and Technology*, No. 59, pp. 925 – 935, 1999.

[22] W. J. Gadja, "A fundamental study of the electromagnetic properties of advanced composite materials", Phase 1 Report RADC-TR-78-158, ADA059029, 1978, online [available] https://apps.dtic.mil/sti/citations/ADA059029

[23] R. H. Knibbs and J.B. Morris, "The effects of fiber orientation on the physical properties of composites", *Composites*, Vol. 5, pp. 209-218, 1974.

[24] V. Volpe, "Estimation of electrical conductivity and electromagnetic shielding characteristics of graphite/epoxy laminates", *Journal of Composite Materials*, Vol. 14, pp. 189 - 198, 1980.

[25] Y. Xue, B. Gu and B. Sun, "Effect of direct current direction on electro-thermal damage of carbon fiber/epoxy plain woven laminates", *Composite Structures*, Vol. 300, 2022, doi: 10.1016/j.compstruct.2022.116197.

[26] M.F. Haider et al, "Nonlinear Anisotropic Electrical Response of Carbon Fiber-Reinforced Polymer Composites", Journal of Composite Materials, Vol. 52, No. 8,pp 1017-1032, doi: 10.1177/0021998317719999.

[27] Misubishi Rayon Co. Ltd., "Dialead", available [online] https://makesat.com/uploads/product_document/37/DIALEAD_EN201609.pdf

[28] Huntsman Advanced Materials, "Araldite LY 5210/Aradur 017/Accelerator DY 070", 2009, [online]. Available: https://www.viba.nl/media/files/tds/tds0000912.pdf

[29] C.E. Jones et al, "Grounding topologies for resilient, integrated composite electrical power systems for future aircraft applications", *IEEE/AIAA Electric Aircraft Symposium*, 2019.
[30] Chau, J.: 'Supplement to M6.11/M7.07 EWISBonding and grounding network for composite structure aircraft', Temasek Polytech, 2018
[31] T. Schroeter and D. Schulz, "The Electrical Aircraft Network – Benefits and Modifications", *IEEE Trans. on Aerospace and Electronic Systems*, Vol. 49, No. 1, 2013, doi: 10.1109/TAES.2013.6404098.
[32] "IEEE Recommended practice for grounding of industrial and commercial power systems", *IEEE Std 142-2007*, 2007.
[33] T. Baldwin and F. Renovich, "Analysis of Fault Locating Signals for High-Impedance Grounded Systems", *IEEE Trans. Industry Applications*, Vol.38, no. 3, 2002. Doi: 10.1109/TIA.2002.1003434
[34] G. Skibinski et al, "Part II: Application Guidelines for High Resistance Grounding of Low-Voltage Common AC-Bus and Common DC-Bus PWM Drive Systems", *IEEE Trans. on Industry Applications*, Vol. 51, No. 2, pp. 1385 – 1397, 2015, doi: 10.1109/TIA.2014.2363074
[35] J.C. Das and R. H. Osman, "Grounding of AC and DC Low-Voltage and Medium-Voltage Drive Systems", IEEE Trans. on Industry Applications, Vol. 34. No.1, pp. 205 – 216, doi: 10.1109/28.658747.

Dr Catherine E. Jones received the MEng (Hons) degree in Electronics and Electrical Engineering from the University of Glasgow, Glasgow, UK, in 2003, and the PhD in Electrical Engineering from the University of Manchester, Manchester, UK, in 2006. She is currently a Chancellor's Fellow (Lecturer) with the Institute for Energy and Environment, University of Strathclyde, Glasgow, UK. Her research interests include design of compact, resilient power system architectures for weight and safety critical applications, and the design interface between electrical and non-electrical systems to optimise power density.

Mark Higgins received the M.Eng degree in Electrical and Mechanical Engineering from the University of Strathclyde, Glasgow, U.K., in 2021, where he is currently pursuing the Ph.D. degree with the Rolls-Royce University Technology Centre for Electrical Power Systems. His research interests include electrical characterisation of CFRP, and resilient integration of electrical power systems with composite structures.

Muhammad Hijaaj Tahir received his B.Sc. and M.Sc. degrees in Electrical Engineering from the HITEC University, Pakistan, in 2016 and 2020, respectively. He is currently pursuing a Ph.D. in Electronic and Electrical Engineering at the University of Strathclyde, Glasgow, U.K, within the Rolls-Royce University Technology Centre for Electrical Power Systems. His research interests include design methodologies for multifunctional composite materials for aircraft.

Dr Patrick Norman is a Reader in Aerospace Electrical Systems within the Department of Electronic and Electrical Engineering at UoS, where he also received his BEng and PhD degrees. He is the academic lead for Aerospace-Electrical Systems research team, building on 20 years of research experience in the field of more-and hybrid-electrical aircraft systems. He is internationally recognised for his work on aircraft power systems modelling, design and protection. His research into new power system architectures and design methodologies has been adopted by a number of leading UK aerospace industries and he holds three patents on protection methods for compact DC aircraft power systems. He has also published over 80 technical papers in leading journals and conferences.

Prof. Graeme M. Burt (M'95) received the B.Eng. degree in electrical and electronic engineering, and the Ph.D. degree in fault diagnostics in power system networks from the University of Strathclyde, Glasgow, U.K., in 1988 and 1992, respectively. He is a distinguished professor of electrical power systems engineering in the Department of Electronic and Electrical Engineering at the University of Strathclyde, UK, where he directs the Institute for Energy and Environment. His research interests span decentralised and hybrid energy systems, electrification of propulsion, DC and hybrid power distribution, and experimental validation of advanced power systems.